

# Equivalence between State-Space Stability Analysis and Generalized Nyquist Criterion with Frequency Dynamics Included

Pablo Rodríguez-Ortega, Javier Roldán-Pérez, *Member, IEEE*, and Milan Prodanović, *Member, IEEE*

**Abstract**—Stability of power electronic converters connected to power grids is commonly assessed by using the impedance criterion. On the contrary, stability of power grids is typically analysed by using network state-space representation and system eigenvalues. It has been already reported in the literature that the impedance criterion may lead to erroneous results if the dynamics of the grid frequency is not taken into consideration. Meanwhile, the eigenvalue analysis is still considered as a reliable method for finding instabilities. However, the equivalence between these two methods (impedance criterion with frequency dynamics included and eigenvalue analysis) has not been thoroughly studied before. In this paper, the impedance method with frequency dynamics included is compared with the conventional eigenvalue analysis for a system fully based on electronic interfaces. Analytical expressions that link both methods are provided, showing that they are identical under certain conditions. Then, both methods are applied to a system based on a grid-forming and a grid-following converter. The results obtained from real-time simulations performed in OPAL-RT are used to validate the theoretical developments and main contributions of this work.

**Index Terms**—Impedance criterion, eigenvalue analysis, frequency dynamics, grid-forming, grid-following.

## I. INTRODUCTION

Stability assessment based on eigenvalue analysis is commonly used in the power systems field. The application of this method requires detailed information about all the system elements, including hardware and control parameters. This method can be readily applied in conventional power systems since the number of generators is relatively small and their parameters are well known. However, most of the new generators are connected to the grid by using electronic interfaces that are more difficult to model [1]. An alternative method for stability assessment in systems dominated by electronic interfaces is the impedance criterion. With this method, only the frequency response of the grid output impedance is required. The latter can be obtained by using either numerical simulations or measurements from the real power grid. Therefore, detailed information about the grid is not necessary. In recent years this fact has motivated researchers to actively contribute to this field, even though the stability criteria are less obvious and more difficult to evaluate [2, 3].

The impedance criterion was firstly introduced by Middlebrook in order to study the stability of interconnected

dc-dc converters [4]. Later, the basic criterion was adapted by Jian Sun in order to study ac converters connected to a grid [5]. Since these initial developments, many researchers have advanced this fundamental theory and proposed new ways to improve the stability analysis [6–11]. In parallel, the tools required to perform these analyses such as impedance identification techniques based on measurements have also received important attention [12–15].

Modern power systems are integrating a large number of renewable energy sources via power electronics converter interfaces that, as a consequence, leads to reduced levels of system inertia [16–18]. Therefore, the frequency dynamics have gained importance as it has been already shown that it has important implications on the stability [19, 20]. One important shortcoming of the impedance criterion is that despite accounting for variations of the frequency operating point, it does not account for frequency dynamics [21]. Several recent publications have shown that is possible to include the frequency dynamics in the impedance criterion (e.g., including the PLL dynamics [22–25]). An alternative impedance representation that includes the frequency dynamics was introduced by Wen *et al.* [26]. The authors presented an identification method to obtain the frequency dynamics. Also, they proposed, in a general way, a mathematical formulation that takes into account the frequency dynamics in the impedance stability criterion. Results showed that accuracy greatly increased compared to the original impedance criterion. Several efforts have been made to determine how reliable is the impedance method compared to the well-known eigenvalue stability analysis. In particular, M. Amin *et al.* [27] compared the impedance and the eigenvalue methods for a system consisting of a two-terminal VSC-HVDC interconnection. Other studies have demonstrated cases where the impedance criterion featured important deficiencies. In particular, L. Fan *et al.* [28] revealed issues with the accuracy of the impedance criterion. In that work, the stability analysis was performed based on the eigenvalue and the impedance methods, for two different cases. The case studies included a grid-connected converter, and different values of the grid-impedance were used to test and assess its impact on the system stability. However, frequency dynamics were not considered. Remarkably, to the best of the authors knowledge, a closed-form expression that links the impedance criterion including the frequency dynamics and the eigenvalue method has not been presented before.

In this paper, the impedance-based assessment method with the frequency dynamics included is compared to the eigenvalue method for the power grids fully based on electronic interfaces. The impedance criterion with the frequency dynamics included

P. Rodríguez-Ortega, J. Roldán-Pérez and M. Prodanović are with IMDEA Energy Institute, Madrid Spain. email: pablo.rodriguez@imdea.org. This work is financially supported by research project PROMINT-CAM (S2018/EMT-4366) from Community of Madrid and from the Spanish Government through Juan de la Cierva Incorporación program (IJC2019-042342-I). In addition to that, the authors would like to acknowledge the support from the research project FLEXENER funded by the Research Program Misiones CDTI. P. Rodríguez-Ortega is also with Alcalá de Henares University.

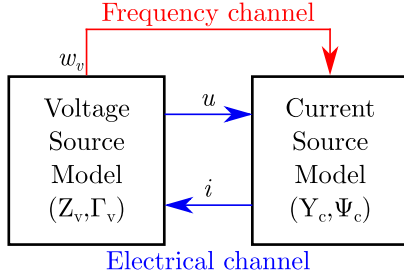


Fig. 1. Equivalent model of the system under study.

(that will be called “extended impedance criterion” from now on) will be introduced first. Then, closed-form formulas that link state-space models and impedance models will be derived. The proposed developments will be validated by using a test case consisting of a grid-forming and a grid-following converter. In this test case, the relative influence of frequency dynamics will be firstly analysed. Then, the system eigenvalues analysis and the generalised Nyquist criterion will be applied. Real-time simulations will be performed by using OPAL-RT and the stability predictions will be verified.

## II. EXTENDED IMPEDANCE CRITERION

In this section, the impedance criterion with the frequency dynamics included is presented. It is based on the theory presented in [26], although it has some variations in the annotation in order to adapt it to proposed developments.

### A. System Modelling

Fig. 1 shows the block diagram that is used in this work to model interconnected devices. The first device (on the left) is called voltage source model (VSM). The outputs are the voltage and the frequency while the current is an input. The other device (on the right) is called current source model (CSM). In this model, the output is the current while the voltage and frequency are the inputs. In the following sections, the VSM is used to model a grid-forming device and the CSM is used to model a grid-following device. These roles are selected here for simplicity. However, other alternative configurations are possible (e.g., modelling a droop based grid-forming device with a CSM, etc.).

The CSM current depends on an admittance plus the contribution of the frequency dynamics:

$$\mathbf{I}^{dq}(s) = \mathbf{Y}_C(s)\mathbf{U}^{dq}(s) + \mathbf{\Psi}_C(s)\Omega_V(s), \quad (1)$$

where subscript  $V$  refers to VSM and  $C$  refers to CSM. The frequency of the VSM is a scalar quantity and is denoted with  $\omega_V$  in the time domain and  $\Omega_V(s)$  in the Laplace domain. It is a scalar. The voltage is named  $\mathbf{U}^{dq}(s)$  and the current is named  $\mathbf{I}^{dq}(s)$ . Both are the representations in the Laplace domain of the space vectors in  $dq$ :

$$\mathbf{I}^{dq}(s) = \begin{bmatrix} I^d(s) \\ I^q(s) \end{bmatrix}, \quad \mathbf{U}^{dq}(s) = \begin{bmatrix} U^d(s) \\ U^q(s) \end{bmatrix}. \quad (2)$$

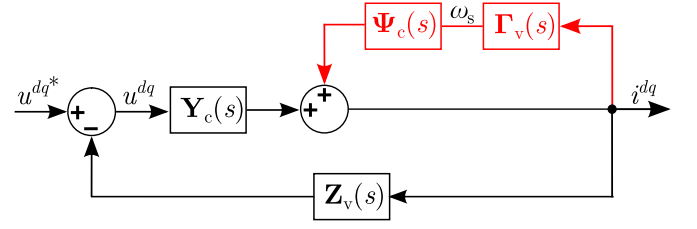


Fig. 2. System Block diagram to help understanding the extended impedance criterion. (black) The electrical impedance considering (red) the frequency dynamics.

In (1),  $\mathbf{Y}_C(s)$  is the admittance matrix and  $\mathbf{\Psi}_C(s)$  is called frequency-admittance vector. These are defined as follows:

$$\mathbf{Y}_C(s) = \begin{bmatrix} Y_C^{dd}(s) & Y_C^{dq}(s) \\ Y_C^{qd}(s) & Y_C^{qq}(s) \end{bmatrix}, \quad \mathbf{\Psi}_C(s) = \begin{bmatrix} \Psi_C^d(s) \\ \Psi_C^q(s) \end{bmatrix}. \quad (3)$$

The units of the terms inside the admittance matrix are Siemens (S) and the units of the terms inside the frequency-admittance vector are A/(rad/s).

For the case of the VSM, it is defined as follows:

$$\mathbf{U}^{dq}(s) = \mathbf{Z}_V(s)\mathbf{I}^{dq}(s), \quad (4)$$

$$\Omega_V(s) = \mathbf{\Gamma}_V(s)\mathbf{I}^{dq}(s), \quad (5)$$

where

$$\mathbf{Z}_V(s) = \begin{bmatrix} Z_V^{dd}(s) & Z_V^{dq}(s) \\ Z_V^{qd}(s) & Z_V^{qq}(s) \end{bmatrix}, \quad \mathbf{\Gamma}_V(s) = \begin{bmatrix} \Gamma_V^d(s) & \Gamma_V^q(s) \end{bmatrix}. \quad (6)$$

The impedance matrix is called  $\mathbf{Z}_V(s)$  and its units are Ohms. The other matrix is  $\mathbf{\Gamma}_V(s)$  and in this work it is referred as the frequency-impedance matrix. The units of the terms inside this matrix are (rad/s)/A. The frequency-impedance and frequency-admittance are concepts similar to the impedance and admittance in electrical circuits, yet adapted to represent the frequency dynamics.

### B. Development of the Stability Criterion

The systems presented in (1), (4) and (5) can be merged together, leading to the block diagram presented in Fig. 2. The black elements represent the electrical impedance and the red elements represent the frequency dynamics. The dynamic equation that links the current and the voltage is:

$$[\mathbf{I} + \mathbf{Y}_C(s)\mathbf{Z}_V(s) - \mathbf{\Psi}_C(s)\mathbf{\Gamma}_V(s)]\mathbf{I}^{dq}(s) = \mathbf{Y}_V(s)\mathbf{U}^{dq}(s), \quad (7)$$

where  $\mathbf{I}$  is the identity matrix of dimension two. This system will be stable in closed-loop if 1) there are no unstable pole-zero cancellations and 2) the roots of:

$$\mathbf{H}(s) = \mathbf{I} + \mathbf{Y}_C(s)\mathbf{Z}_V(s) - \mathbf{\Psi}_C(s)\mathbf{\Gamma}_V(s) \quad (8)$$

are placed in the left-half side of the complex plane [29].

The equivalent open-loop transfer function matrix (i.e., minor loop) then becomes the following function:

$$\mathbf{L}(s) = \mathbf{Y}_C(s)\mathbf{Z}_V(s) - \mathbf{\Psi}_C(s)\mathbf{\Gamma}_V(s). \quad (9)$$

Closed-loop stability can be guaranteed if the open-loop system fulfils the generalized Nyquist criterion (GNC). This means that each of the eigenvalues of  $\mathbf{L}(s)$  should fulfil the

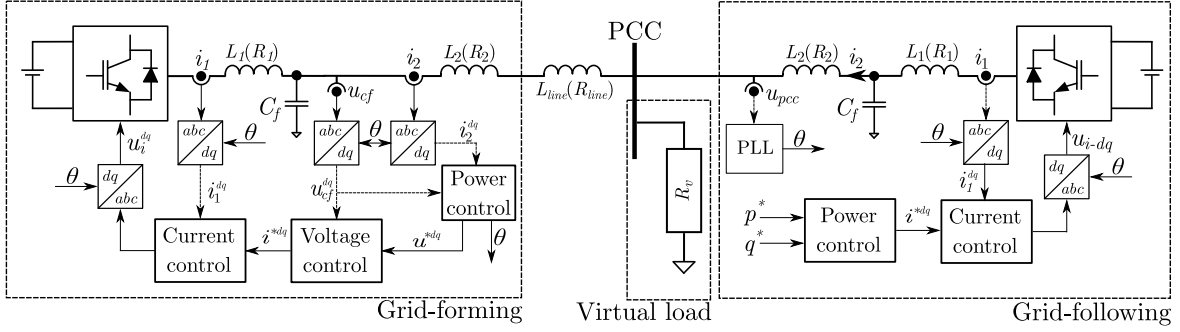


Fig. 3. Test system used for the validation of the extended impedance criterion. It includes a grid-forming converter, a grid-following converter and a load.

Nyquist criterion for SISO systems. The eigenvalue loci are defined as follows:

$$\det(I + \mathbf{L}(j\omega)) = \prod_i (1 + \lambda_i(j\omega)). \quad (10)$$

In this extended version of the impedance criterion, it is easy to see that setting  $\Psi_C(s)\Gamma_V(s) = \mathbf{0}$  leads to the standard impedance criterion. Here, the effects of the impedance dynamics and the frequency dynamics are clearly separated. In the following section, it will be shown that this allows to study separately the impact of each channel on the stability of the whole system. Moreover, it allows a simpler interconnection of models of different devices.

### III. IMPEDANCE AND STATE-SPACE MODELLING

In order to verify the extended impedance criterion, the test system is modelled by using both the state-space and the impedance methods.

#### A. Test System Description

The extended impedance criterion will be validated by using the test system presented in Fig. 3. This system consists of a grid-forming and a grid-following converter. These devices are modelled as a VSM and a CSM, respectively. The grid-forming device includes an internal current controller, an external voltage controller and standard voltage and frequency droops [30]. The grid-following converter includes a current controller implemented in a synchronous reference frame (SRF). The SRF is synchronised with the  $d$ -axis voltage component at the point of common coupling (PCC). A phase-locked loop (PLL) with the standard configuration is used for that purpose [31]. The specific values of hardware elements and control parameters can be found in Section VI-A.

#### B. Impedance-Based Modelling

The impedance circuit used for the system modelling is shown in Fig. 4. In that figure,  $Z_{gfr}^{dq}(s)$  is the impedance of the grid-forming converter,  $Z_{line}^{dq}(s)$  is the impedance of the line,  $Z_{load}^{dq}(s)$  is the impedance of a virtual load,  $Z_V^{dq}(s)$  is the impedance of the grid-forming converter plus the line and the virtual load, and  $Y_C^{dq}(s)$  is the admittance of the grid-following converter. The values of these impedances/admittances are obtained using measurements, by applying the procedure described in [32]. The identification

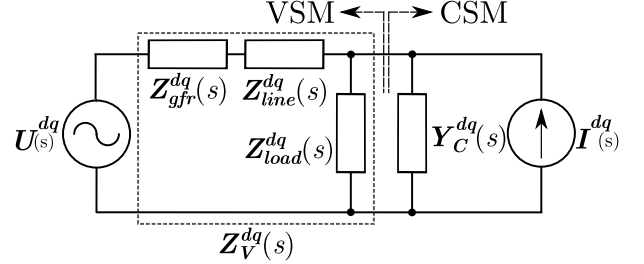


Fig. 4. Small-signal representation of the system based on impedances.

method is performed frequency-by-frequency. In particular, for each frequency, two tones are injected to identify the impedance/admittance, and one tone to identify the frequency dynamics. Then, the GNC is used to analyse the stability limits of the interconnected devices.

#### C. VSM State-Space Modelling

The linearised state-space model of the VSM is developed here. Then, it is linked with the impedance and the frequency-impedance concepts presented in (4) and (5). The detailed mathematical procedure to obtain the state-space matrices can be found in the literature [30]. In this paper, only the most relevant steps will be discussed. The state-space model of the grid-forming converter with the line-impedance has the following structure

$$\begin{aligned} [\Delta \dot{x}_V] &= A_V [\Delta x_V] + B_{u-V} [\Delta u^{dq}] \\ &\quad + B_{\omega-V} [\Delta \omega_V], \\ \begin{bmatrix} \Delta \omega_V \\ \Delta i^{dq} \end{bmatrix} &= C_V [\Delta x_V], \end{aligned} \quad (11)$$

where  $x_V$  represents the states of the VSM,  $u^{dq}$  is the input voltage in  $dq$  (i.e., PCC voltage),  $\omega_V$  is the frequency of the grid-forming converter and  $i^{dq}$  is the output current in  $dq$ . The symbol  $\Delta$  stands for “incremental” (i.e., small-signal modelling). The matrices  $A_V$ ,  $B_{u-V}$ ,  $B_{\omega-V}$  and  $C_V$  can be calculated as described in [30]. The impedance of the VSM ( $Z_V(s)$ ) can be derived from (11):

$$Z_V(s) = [C_V(sI - A_V)^{-1}B_{u-V}]^{-1}. \quad (12)$$

However, the frequency-impedance dynamics ( $\Gamma_V(s)$ ) cannot be directly derived from (11). This happens because the current should be an input so as to model the device as a VSM, like

in (5). However, in (11)  $\Delta i_v^{dq}$  is an output. To solve this issue, a virtual resistor can be added:

$$\Delta u^{dq} = R_v \cdot (\Delta i_v^{dq} - \Delta i^{dq}), \quad (13)$$

where  $i_v^{dq}$  is a virtual current. After adding this new equation to the state-space representation in (11), the following result is obtained:

$$\begin{aligned} [\dot{\Delta x}_M] &= A_M [\Delta x_M] + B_{i-M} [\Delta i^{dq}], \\ [\Delta \omega_V] &= C_M [\Delta x_M], \end{aligned} \quad (14)$$

where

$$\begin{aligned} A_M &= A_V + B_{u-V} \cdot R_v, \\ B_{i-M} &= B_{u-V} \cdot R_v, \\ C_M &= C_V. \end{aligned} \quad (15)$$

Subindex  $M$  stands for “modified”, and then  $x_M$  represents the modified states of the VSM. Then, the frequency-impedance vector can be calculated as follows:

$$\Gamma_V(s) = C_M(sI - A_M)^{-1} B_{i-M}. \quad (16)$$

1) *CSM State-Space Modelling*: In this subsection, the state-space model of the grid-following converter is presented. Only the most relevant steps are presented since the details can be found in the literature [33]. Then, the admittance matrix and the frequency-admittance vector are calculated from the state-space model.

The state-space model of the grid-following converter is as follow:

$$\begin{aligned} [\dot{\Delta x}_C] &= A_C [\Delta x_C] + B_{pq-C} [\Delta PQ] + B_{u-C} [\Delta u^{dq}] \\ &\quad + B_{\omega-C} [\Delta \omega_C], \\ [\Delta i^{dq}] &= C_C [\Delta x_C], \end{aligned} \quad (17)$$

where  $x_C$  are the states of the CSM model. Matrices  $A_C$ ,  $B_{u-C}$ ,  $B_{\omega-C}$  and  $C_C$  can be calculated as described in [33].

Therefore, admittance matrix  $Y_C(s)$  and frequency-admittance vector  $\Psi_C(s)$  can be represented as follows:

$$Y_C(s) = C_C(sI - A_C)^{-1} B_{u-C} \quad (18)$$

and

$$\Psi_C(s) = C_C(sI - A_C)^{-1} B_{\omega-C}. \quad (19)$$

2) *State-Space Model of the Whole System*: The full state-space model including the grid-forming converter, the grid-following converter and the virtual load is presented in here. For that purpose, the models of the VSM and the CSM should be merged together, as explained in [30]. The following result is obtained:

$$\begin{aligned} [\dot{\Delta x}_{SYS}] &= A_{SYS} [\Delta x_{SYS}] + B_{SYS} [\Delta PQ], \\ [\Delta i^{dq}] &= C_{SYS} [\Delta x_{SYS}]. \end{aligned} \quad (20)$$

Subindex  $SYS$  stands for “power system”,  $x_{SYS}$  represents the states of the VSM and the CSM, and the matrices  $A_{SYS}$ ,  $B_{SYS}$  and  $C_{SYS}$  can be obtained as in [30].

In (20), the system is stable if all the eigenvalues of  $A_{SYS}$  are placed in the left-hand side of the complex plane. Also, from the expressions calculated in the Laplace domain in (12) and (16) for the VSM and, (18) and (19) for the CSM, the

system is stable if  $L(s)$  fulfils the GNC. One should note that in both cases the system small-signal dynamics were calculated without neglecting any dynamic effect. Therefore, if there are not unstable pole-zero cancellations, both criteria should provide similar results regarding the system stability.

#### IV. EQUIVALENCE BETWEEN IMPEDANCE AND STATE-SPACE REPRESENTATION

The state-space and impedance-based models developed in the previous section are compared in order to show the equivalence of both stability analysis methods and the impact of the frequency dynamics in the system.

##### A. Comparison between Impedance and State-Space Models

The VSM and CSM are studied here. For both cases, the results obtained using the impedance methodology will be compared to those obtained using the state-space methodology. First, Fig. 5 and Fig. 6 show the response in frequency domain of the admittance and the frequency-admittance of the VSM, respectively. The results for the state-space method are presented in blue and the results for the impedance method are presented in red. It can be seen that in both cases the modelling approaches lead to similar results. Results show an excellent match below 100 Hz, while in the range of 100 Hz to 1 kHz some small differences can be observed. These small differences are caused by the method used to identify the impedances (that is accurate, but not perfect [34]). Fig. 7 and Fig. 8 show the admittance and the frequency admittance of the CSM. Results follow the same trend with those presented for the VSM. Based on these results, it is assumed from now on that the extended impedance criterion is valid, and that the tools used in this work are sufficiently accurate to be applied to the case under study. An application to systems with multiple interactions between different converter-devices is also possible, although other considerations should be taken into account [23].

##### B. Impact of Frequency Dynamics on the GNC

The objective in this Section is to determine the impact of frequency dynamics on the stability of the interconnected system. This will be achieved by analysing the eigenvalues of the minor loop  $L(s)$  for  $s = j\omega$ , with  $\omega \in (-\infty, \infty)$ . As  $L(j\omega)$  is a square matrix of second order, then it has two eigenvalues:  $\lambda_1(j\omega)$  and  $\lambda_2(j\omega)$ . These eigenvalues will be depicted in polar coordinates so that the GNC can be applied (see Section II-B for details on the GNC). Bode diagrams will be used to showcase the effect of the frequency dynamics at specific frequencies, since it is easier to understand its behaviour. In the following expressions, if the frequency dynamics are not considered (i.e.,  $L'(s) = Y_C(s)Z_V(s)$ ), then the eigenvalues will be named  $\lambda'_1(j\omega)$  and  $\lambda'_2(j\omega)$ . In addition, the frequency dependency of eigenvalues will be dropped from now on for simplicity the presentation.

Fig. 9 shows the Bode diagram of the system eigenvalues, with and without the contribution of the frequency dynamics. From a general perspective, there are no important differences. However, there is an important mismatch in the phase at

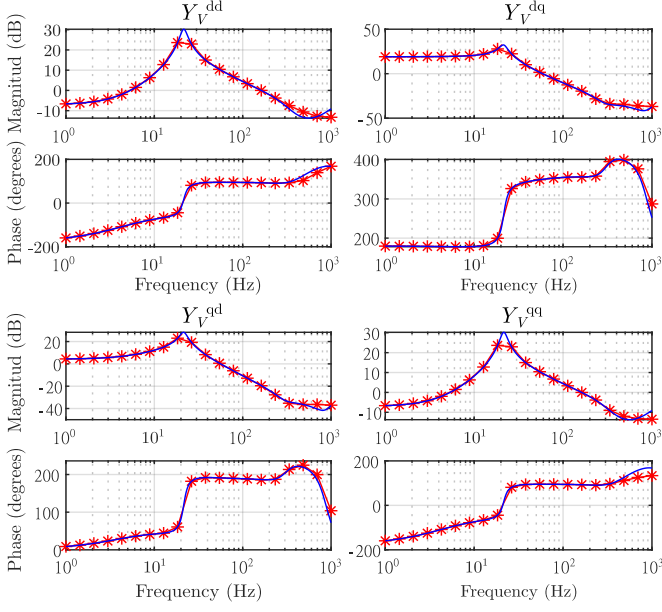


Fig. 5. Frequency domain identification of the grid-forming admittance.

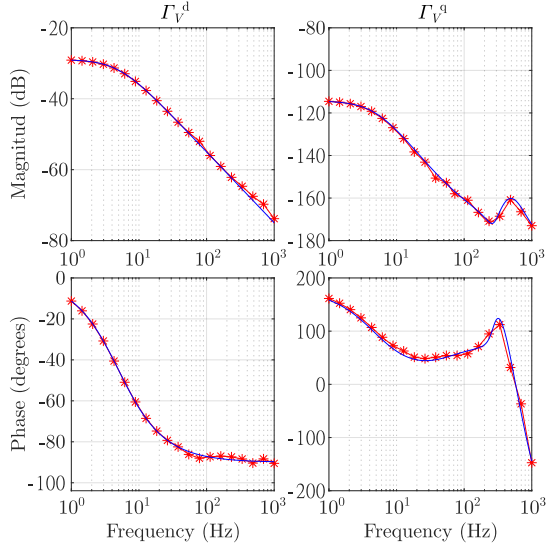


Fig. 6. Frequency domain identification of the frequency dynamics for the grid-forming converter.

the frequencies around 1 Hz. The stability of the system is assessed by checking if the magnitude is above (unstable) or below (stable) 0 dB for the frequency when the phase crosses  $-180^\circ$ . The phase of the first eigenvalue never crosses  $-180^\circ$ , so as it is always stable and this eigenvalue can be neglected. In the other case, the phase of the second eigenvalue is shifted to lower frequencies when the frequency dynamics are considered. This fact provokes relevant changes to the system stability, since the magnitude when the phase crosses  $-180$  degrees is significantly modified. The system changes from being unstable to stable. Therefore, the bode diagram is considered of interest for finding at what frequency the system becomes unstable.

The implications of these differences can be highlighted better by using the Nyquist plot. Fig. 10 shows the Nyquist plot for the two eigenvalues. The unit circle is marked using black colour. It can be observed that the effects of frequency

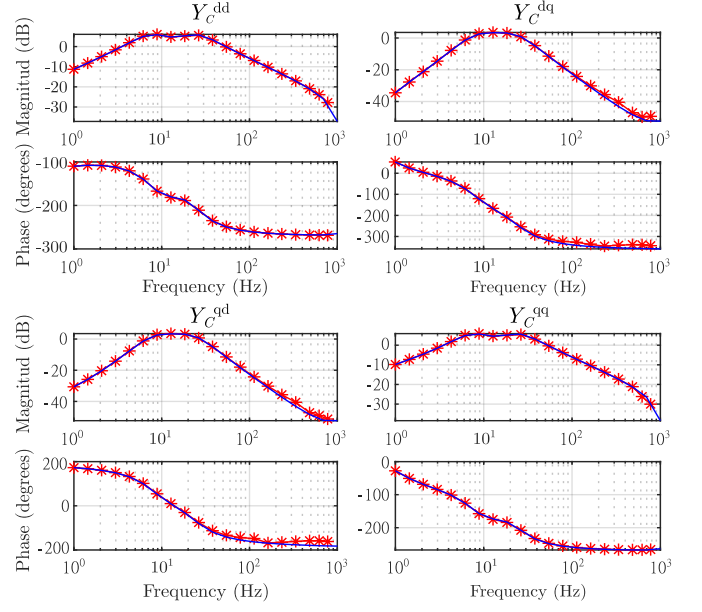


Fig. 7. Frequency domain identification of the grid-following admittance.

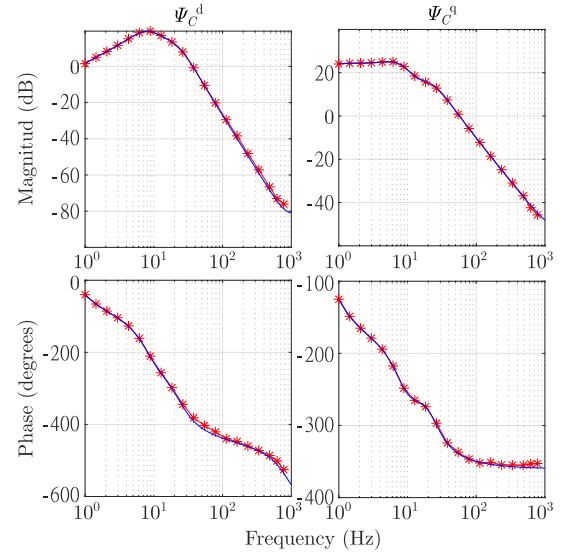


Fig. 8. Frequency domain identification of the frequency dynamics for the grid-following converter.

dynamics become clearly visible in the Nyquist plots. For  $\lambda_1$ , despite the differences, these do not affect the system stability since the phase is always far from  $-1$ . For the case of  $\lambda_2$  there are also important differences. For high frequencies,  $\lambda_2$  and  $\lambda_2'$  do not differ. However, at low frequencies, the crossing of  $-1$  is significantly different. Indeed, on the one hand, if the frequency dynamics is taken into consideration ( $\lambda_2$ ), the point  $-1$  is not encircled and the full system is (theoretically) stable. On the other hand, if the frequency dynamics are not considered ( $\lambda_2'$ ), the GNC predicts the system will be unstable. From these results, it can be concluded for this particular case study that:

- 1) In this particular case, stability in the low-frequency range is mainly linked to one eigenvalue.
- 2) The GNC without including the frequency dynamics yields erroneous stability assessment.

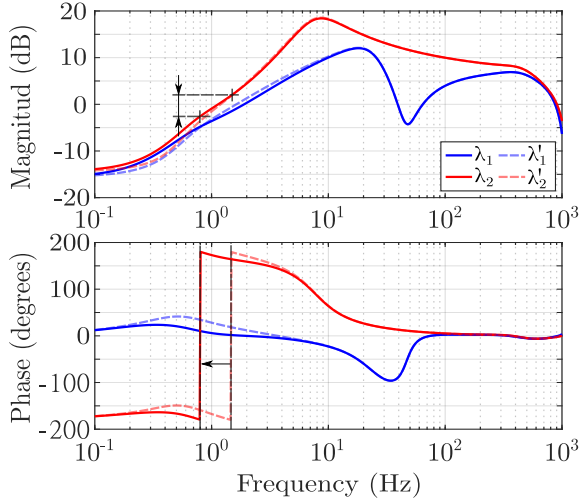


Fig. 9. Bode diagram of  $\lambda_1$ ,  $\lambda_1'$ ,  $\lambda_2$  and  $\lambda_2'$ , for the studied system.

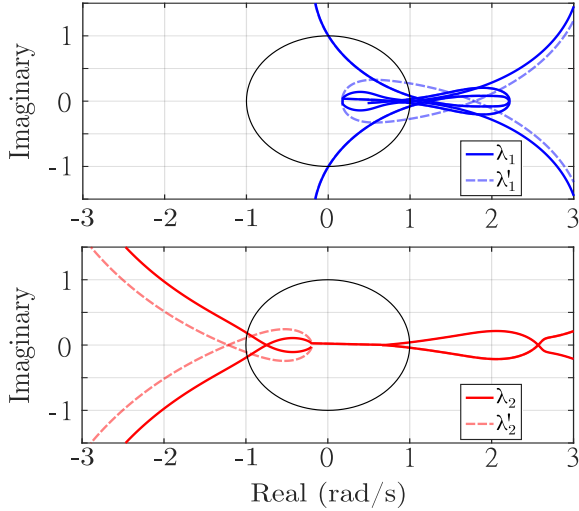


Fig. 10. Nyquist plot of the eigenvalues of the minor loop, with and without the frequency dynamics.

## V. STABILITY ANALYSIS

In this section, the extended impedance criterion will be applied to the system of Fig. 3. In particular, the impact of the current controller bandwidth of the CSM, the PLL bandwidth and the line impedance will be studied in detail. The significance of the frequency dynamics is particularly highlighted. Finally, the results obtained by using the extended impedance criterion are compared to those obtained by the eigenvalue method.

### A. Current-Controller Bandwidth

Fig. 11 (a) shows the Bode diagram of  $\lambda_1$ ,  $\lambda_1'$ ,  $\lambda_2$  and  $\lambda_2'$  when the bandwidth of the current controller of the grid-following converter decreases. The line impedance is kept constant at  $L = 7$  mH and  $R = 0.4$   $\Omega$ , the PLL bandwidth is  $2\pi$  rad/s and the bandwidth of the current-bandwidth decreases from 100 to 70 rad/s. In this case, the magnitude gain of  $\lambda_1$  and  $\lambda_2$  increases. The impact on  $\lambda_1$  is not important as the system phase is far from crossing  $-180$  degrees. However, it is important for  $\lambda_2$  since it affects the gain at which the

phase crosses  $-180$  degrees. Fig. 12 (a) shows a zoom of the Nyquist plot for the relevant cases of  $\lambda_2$  around  $-1$ . It can be seen that the system clearly becomes unstable when the bandwidth is set to 70 rad/s. Moreover, it can be seen that the impact of the frequency dynamics is significant. Indeed, for the first value of the bandwidth, the extended stability criterion suggests that the system is stable. However, the simplified impedance criterion implies the system is unstable regardless of the value of the bandwidth. Fig. 13 (a) shows the system eigenvalues for this specific case. It can be seen that, for the first values the system is stable and when the value reaches the 70 rad/s, the system clearly becomes unstable. This is in accordance with the extended impedance criterion.

### B. PLL Bandwidth

In this case, the bandwidth of the current controller is kept constant at 100 rad/s and the line parameters are 7 mH and 0.4  $\Omega$ . The PLL bandwidth is increased from  $2\pi$  to  $4 \cdot 2\pi$  rad/s. Fig. 11 (b) shows the Bode diagram of  $\lambda_1$  and  $\lambda_2$ , with and without the contribution of the frequency dynamics. It can be seen that the effect of the PLL bandwidth is relevant across a narrow frequency range (from 0.3 Hz to 3 Hz). As in the previous case,  $\lambda_1$  does not have any relevant influence on the stability limits, while  $\lambda_2$  is important. Fig. 12 (b) shows the Nyquist plot for the same cases studied in Fig. 11 (b), while Fig. 13 (b) shows the eigenvalues of the closed-loop system. By observing the results, the conclusions are similar compared to the previous case: when the frequency dynamics are included, the system becomes better damped.

### C. Line Impedance

In this case, the line impedance will be modified while the rest of parameters will be kept constant. The current-bandwidth of the grid-following converter is fixed to 70 rad/s and the PLL bandwidth to  $2\pi$  rad/s. The line impedance is increased from 3 mH and 0.2  $\Omega$  to 7 mH and 0.4  $\Omega$ , respectively. Fig. 11 (c) shows the Bode diagram of the impedance, Fig. 12 (c) shows the Nyquist plot of the most relevant  $\lambda_2$  cases from  $L = 4$  mH and  $R = 0.25$   $\Omega$  to 6 mH and 0.325  $\Omega$  and Fig. 13 (c) shows the system eigenvalues. Clearly, the results show the same trends as those presented in previous sections.

## VI. REAL-TIME SIMULATION RESULTS

### A. Parameters

In order to validate the theoretical analyses, real-time simulations have been performed. For that purpose, a non-linear model was developed using Matlab/Simulink and its simPowerSystems toolbox. Then, the three simulation cases presented in the previous Section were implemented and tested in real time using OPAL-RT. The nominal power, voltage and frequency of the system were set to 15 KW, 400 V and 50 Hz, respectively. The rest of the hardware and control parameters can be found in [30, 35]. The results presented in the following section confirm the stability predictions made in previous sections.



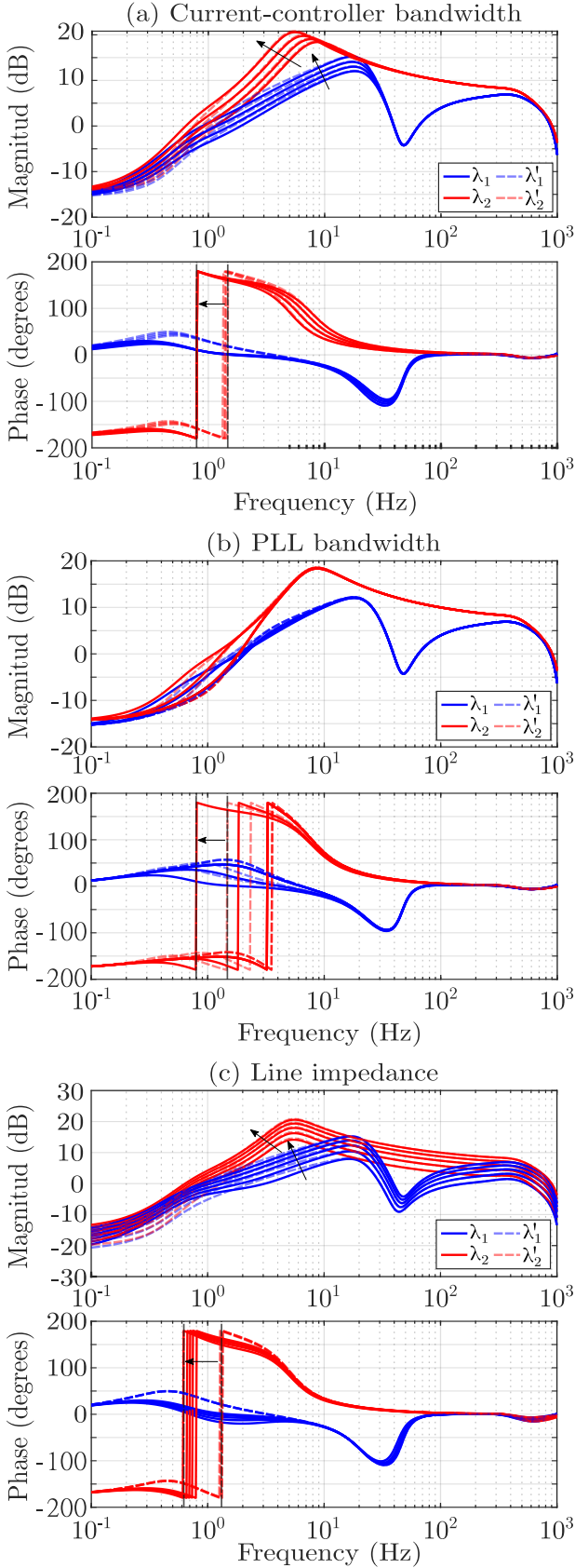


Fig. 11. Bode diagram of  $\lambda_1$ ,  $\lambda'_1$ ,  $\lambda_2$  and  $\lambda'_2$  to analyse the effects of changing the parameters (a) Current-controller gain (b) PLL bandwidth and (c) line-impedance value.

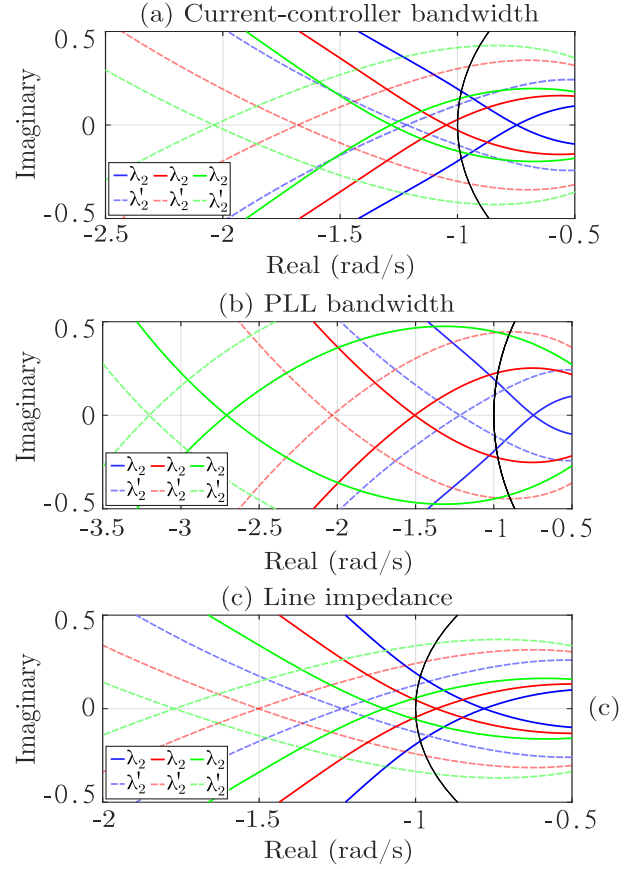


Fig. 12. Nyquist plot of  $\lambda_2$ , for variation of system parameters. (a) Current controller bandwidth, (b) PLL bandwidth and (c) line-inductance.

### B. Real-Time Simulation Results

Fig. 14 shows the real-time simulation results for the three cases studied in the previous section. Time 0 s represents when the system reaches steady state and the different parameters of the study are set. For the first two base cases, the grid inductance is 7 mH and the grid resistance is 0.4  $\Omega$ , the current controller bandwidth is 100 rad/s and the PLL bandwidth is  $2\pi$  rad/s, respectively. Meanwhile, for the third case the current controller bandwidth is 70 rad/s, the PLL bandwidth is  $2\pi$  rad/s, the grid inductance is 4 mH and the grid resistance is 0.25  $\Omega$ . In all the cases, the base case is shown in blue and the case with a modified parameter is depicted in red. It can be seen that the base case is always stable. The original impedance criterion predicted that the system would be unstable for this base case, while the extended impedance criterion and the eigenvalue analysis predict the opposite (see Fig. 12, (a), (b) and (c), in blue). Clearly, the original impedance criterion leads to incorrect results as the system is stable.

1) *Current Controller Bandwidth*: Fig. 14 (a) (red) shows the results obtained when the current-controller bandwidth of the grid-following converter is set to 70 rad/s. In this case, all the criteria indicated the system was going to be unstable and, therefore, results match the predictions. In both the extended impedance criterion and the eigenvalue analysis, the frequency of the instability was around 0.7 Hz. Therefore, the stability analyses and the time domain simulation results are in good

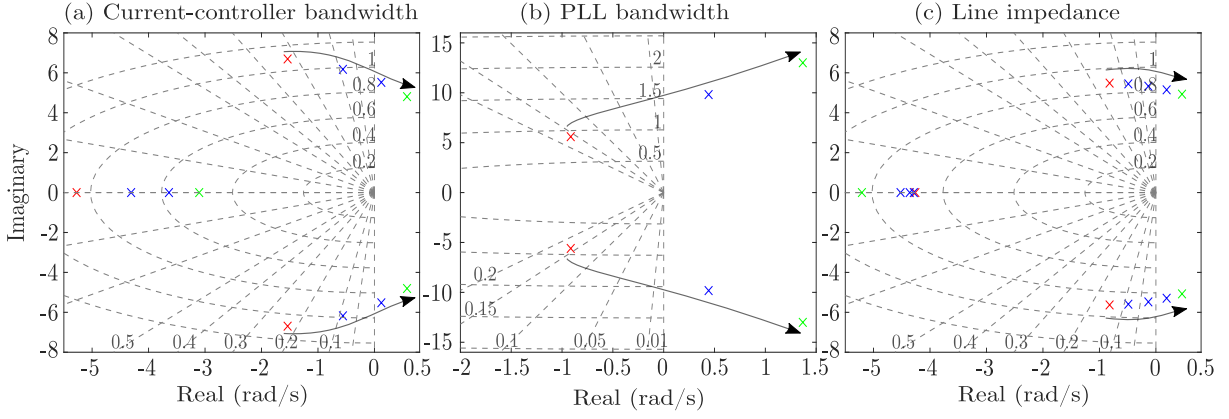


Fig. 13. Trace of the system eigenvalues when the system parameters are modified. (a) Current-controller bandwidth, (b) PLL bandwidth and (c) line-impedance.

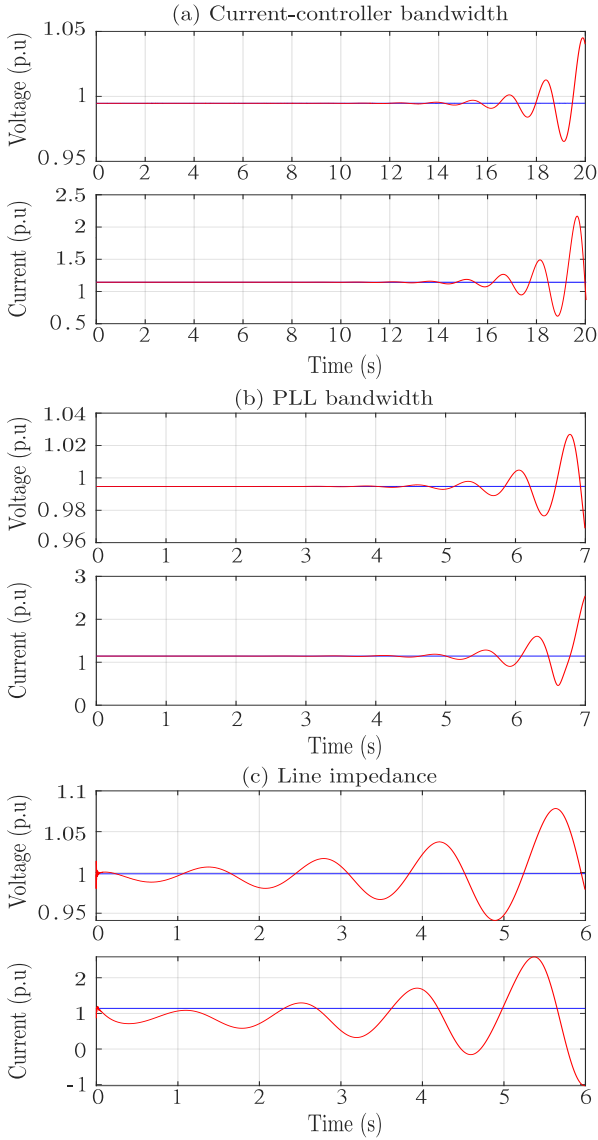


Fig. 14. Time domain simulation for the three cases. Variations in (a) current controller bandwidth, (b) PLL bandwidth and (c) line impedance.

agreement.

2) *PLL Bandwidth*: Fig. 14 (b) (red) shows the simulation results obtained when the PLL bandwidth was set to

$2 \cdot 2\pi$  rad/s. Clearly, the system is unstable. This results was predicted by all the stability criteria. The frequency of the increasing oscillation is around 1.5Hz that is very close to the frequencies estimated by the presented theoretical analyses for the impedance with the frequency dynamics included in Fig. 11 (b) and with the system eigenvalues in Fig. 13 (b).

3) *Line Impedance*: Fig. 14 (c) (red) shows the real-time simulation results obtained when the line-impedance value is increased to  $L = 6$  mH and  $R = 0.35 \Omega$ . The impedance criterion (with and without embedded frequency dynamics) predicts that the system will be unstable. Also, the results from the real-time simulations exhibits an increasing oscillation. The increasing oscillation in the real-time simulation had the frequency of around 0.7 Hz. Fig. 11 (c) shows that this frequency coincides with the frequency at which the phase of 180 degrees is crossed. Also, Fig 13 (c) shows that the frequency of the eigenvalues also match with the frequency of the oscillation.

## VII. CONCLUSION

In this paper, the impact of the grid frequency dynamics on the impedance criterion has been analysed in detail. Closed-form expressions that link both methods have been presented in order to perform the comparison between the stability assessments methods based on the impedance criterion and the eigenvalue analysis. A test system consisting of one grid-following and one grid-forming converter has been used as a benchmark system. Real-time simulations using an OPAL-RT platform were performed in order to validate the main findings.

The obtained results confirmed the impedance modelling and the state-space modelling produce identical responses if the frequency dynamics is included in the impedance model. Only slight differences were appreciated at high frequencies (1 kHz), due to the method used to estimate the impedances. However, if the frequency dynamics is not taken into account, some important mismatches can be produced, especially in the phase at low frequencies (around 1 Hz). These errors in the impedance lead to an inaccurate stability assessment and emphasise the importance of taking into account the grid frequency dynamics.

In addition to that, if the impedance criterion include the frequency dynamics, more conservative assessment results are



produced compared to the case when the frequency dynamics are not considered. However, this conclusion must not be taken as a general rule for all system topologies and configurations.

In future works, it would be of interest to consider more sophisticated identification methods for calculating the impedance and frequency equivalents. Also, it would be of interest to apply the extended impedance criterion to power networks of various sizes and strengths.

#### REFERENCES

- [1] R. H. Lasseter, Z. Chen, and D. Pattabiraman, "Grid-forming inverters: A critical asset for the power grid," *IEEE Journal of Emerging and Selected Topics in Power Electronics*, vol. 8, no. 2, pp. 925–935, 2020.
- [2] J. Sun, "Small-signal methods for ac distributed power systems—a review," *IEEE Transactions on Power Electronics*, vol. 24, no. 11, pp. 2545–2554, 2009.
- [3] X. Yue, X. Wang, and F. Blaabjerg, "Review of small-signal modeling methods including frequency-coupling dynamics of power converters," *IEEE Transactions on Power Electronics*, vol. 34, no. 4, pp. 3313–3328, 2019.
- [4] R. D. Middlebrook and S. Cuk, "A general unified approach to modelling switching-converter power stages," in *1976 IEEE Power Electronics Specialists Conference*, 1976, pp. 18–34.
- [5] J. Sun, "Impedance-based stability criterion for grid-connected inverters," *IEEE Transactions on Power Electronics*, vol. 26, no. 11, pp. 3075–3078, 2011.
- [6] Y. Liao and X. Wang, "Impedance-based stability analysis for interconnected converter systems with open-loop rhp poles," *IEEE Transactions on Power Electronics*, vol. 35, no. 4, pp. 4388–4397, 2020.
- [7] C. Zhang, M. Molinas, A. Rygg, and X. Cai, "Impedance-based analysis of interconnected power electronics systems: Impedance network modeling and comparative studies of stability criteria," *IEEE Journal of Emerging and Selected Topics in Power Electronics*, vol. 8, no. 3, pp. 2520–2533, 2020.
- [8] F. Göthner, R. E. Torres-Olguin, J. Roldán-Pérez, A. Rygg, and O.-M. Midtgård, "Apparent impedance-based adaptive controller for improved stability of a droop-controlled microgrid," *IEEE Transactions on Power Electronics*, vol. 36, no. 8, pp. 9465–9476, 2021.
- [9] Y. Liao, X. Wang, and X. Wang, "Frequency-domain participation analysis for electronic power systems," *IEEE Transactions on Power Electronics*, vol. 37, no. 3, pp. 2531–2537, 2022.
- [10] Y. Zhu, Y. Gu, Y. Li, and T. C. Green, "Participation analysis in impedance models: The grey-box approach for power system stability," *IEEE Transactions on Power Systems*, vol. 37, no. 1, pp. 343–353, 2022.
- [11] L. Orellana, L. Sainz, E. Prieto-Araujo, M. Cheah-Mané, H. Mehrjerdi, and O. Gomis-Bellmunt, "Study of black-box models and participation factors for the positive-mode damping stability criterion," *International Journal of Electrical Power & Energy Systems*, vol. 148, p. 108957, 2023.
- [12] R. Chakraborty, H. Jain, and G.-S. Seo, "A review of active probing-based system identification techniques with applications in power systems," *International Journal of Electrical Power & Energy Systems*, vol. 140, p. 108008, 2022.
- [13] A. Rygg and M. Molinas, "Apparent impedance analysis: A small-signal method for stability analysis of power electronic-based systems," *IEEE Journal of Emerging and Selected Topics in Power Electronics*, vol. 5, no. 4, pp. 1474–1486, 2017.
- [14] H. Gong, X. Wang, and D. Yang, "Dq-frame impedance measurement of three-phase converters using time-domain mimo parametric identification," *IEEE Transactions on Power Electronics*, vol. 36, no. 2, pp. 2131–2142, 2021.
- [15] R. Luhtala, T. Roinila, and T. Messo, "Implementation of real-time impedance-based stability assessment of grid-connected systems using mimo-identification techniques," *IEEE Transactions on Industry Applications*, vol. 54, no. 5, pp. 5054–5063, 2018.
- [16] N. Hatziaziyriou, J. Milanovic, C. Rahmann, V. Ajjarapu, C. Canizares, I. Erlich, D. Hill, I. Hiskens, I. Kamwa, B. Pal, P. Pourbeik, J. Sanchez-Gasca, A. Stankovic, T. Van Cutsem, V. Vittal, and C. Vournas, "Definition and classification of power system stability – revisited and extended," *IEEE Transactions on Power Systems*, vol. 36, no. 4, pp. 3271–3281, 2021.
- [17] F. Blaabjerg, Z. Chen, and S. Kjaer, "Power electronics as efficient interface in dispersed power generation systems," *IEEE Transactions on Power Electronics*, vol. 19, no. 5, pp. 1184–1194, 2004.
- [18] P. Tielens and D. Van Hertem, "The relevance of inertia in power systems," *Renewable and Sustainable Energy Reviews*, vol. 55, pp. 999–1009, 2016.
- [19] A. Adrees, J. Milanović, and P. Mancarella, "Effect of inertia heterogeneity on frequency dynamics of low-inertia power systems," *IET Generation, Transmission & Distribution*, vol. 13, no. 14, pp. 2951–2958, 2019.
- [20] M. Kayikci and J. V. Milanovic, "Dynamic contribution of dfbg-based wind plants to system frequency disturbances," *IEEE Transactions on Power Systems*, vol. 24, no. 2, pp. 859–867, 2009.
- [21] B. Wen, D. Boroyevich, R. Burgos, P. Mattavelli, and Z. Shen, "Small-signal stability analysis of three-phase ac systems in the presence of constant power loads based on measured d-q frame impedances," *IEEE Transactions on Power Electronics*, vol. 30, no. 10, pp. 5952–5963, 2015.
- [22] B. Wen, D. Dong, D. Boroyevich, R. Burgos, P. Mattavelli, and Z. Shen, "Impedance-based analysis of grid-synchronization stability for three-phase paralleled converters," *IEEE Transactions on Power Electronics*, vol. 31, no. 1, pp. 26–38, 2016.
- [23] Y. Gu, Y. Li, Y. Zhu, and T. C. Green, "Impedance-based whole-system modeling for a composite grid via embedding of frame dynamics," *IEEE Transactions on Power Systems*, vol. 36, no. 1, pp. 336–345, 2021.
- [24] B. Hu, H. Nian, M. Li, Y. Xu, Y. Liao, and J. Yang, "Impedance-based analysis and stability improvement of dfbg system within pll bandwidth," *IEEE Transactions on Industrial Electronics*, vol. 69, no. 6, pp. 5803–5814, 2022.
- [25] X. Zhang, Y. Zhang, R. Fang, and D. Xu, "An improved virtual inductance control method considering pll dynamic based on impedance modeling of dfbg under weak grid," *International Journal of Electrical Power & Energy Systems*, vol. 118, p. 105772, 2020.
- [26] S. Wang, Z. Liu, J. Liu, D. Boroyevich, and R. Burgos, "Small-signal modeling and stability prediction of parallel droop-controlled inverters based on terminal characteristics of individual inverters," *IEEE Transactions on Power Electronics*, vol. 35, no. 1, pp. 1045–1063, 2020.
- [27] M. Amin and M. Molinas, "Small-signal stability assessment of power electronics based power systems: A discussion of impedance- and eigenvalue-based methods," *IEEE Transactions on Industry Applications*, vol. 53, no. 5, pp. 5014–5030, 2017.
- [28] L. Fan and Z. Miao, "Admittance-based stability analysis: Bode plots, nyquist diagrams or eigenvalue analysis?" *IEEE Transactions on Power Systems*, vol. 35, no. 4, pp. 3312–3315, 2020.
- [29] S. Skogestad and I. Postlethwaite, *Multivariable feedback control: analysis and design*. John Wiley & sons, 2005.
- [30] N. Pogaku, M. Prodanovic, and T. C. Green, "Modeling, analysis and testing of autonomous operation of an inverter-based microgrid," *IEEE Transactions on Power Electronics*, vol. 22, no. 2, pp. 613–625, 2007.
- [31] F. D. Freijedo, J. Doval-Gandoy, O. Lopez, C. Martinez-Peñalver, A. G. Yepes, P. Fernandez-Comesaña, J. Malvar, A. Nogueiras, J. Marcos, and A. Lago, "Grid-synchronization methods for power converters," in *2009 35th Annual Conference of IEEE Industrial Electronics*, 2009, pp. 522–529.
- [32] B. Wen, D. Boroyevich, R. Burgos, P. Mattavelli, and Z. Shen, "Small-signal stability analysis of three-phase ac systems in the presence of constant power loads based on measured d-q frame impedances," *IEEE Transactions on Power Electronics*, vol. 30, no. 10, pp. 5952–5963, 2015.
- [33] A. Rodríguez-Cabero and M. Prodanovic, "Stability analysis for weak meshed networks with power electronics-based distributed generation," in *IECON 2017 - 43rd Annual Conference of the IEEE Industrial Electronics Society*, 2017, pp. 1569–1574.
- [34] R. Luhtala, T. Roinila, and T. Messo, "Implementation of real-time impedance-based stability assessment of grid-connected systems using mimo-identification techniques," *IEEE Transactions on Industry Applications*, vol. 54, no. 5, pp. 5054–5063, 2018.
- [35] P. Rodríguez-Ortega, J. Roldán-Pérez, and M. Prodanovic, "Multivariable-controlled shunt compensator for damping subsynchronous interactions in electrical distribution networks," *IEEE Transactions on Smart Grid*, pp. 1–1, 2023.